

Ballistic Aggregation in Systems of Inelastic Particles: Cluster growth, structure and aging

Subhajit Paul and Subir K. Das*

Theoretical Sciences Unit, Jawaharlal Nehru Centre for Advanced Scientific Research, Jakkur P.O, Bangalore 560064, India

(Dated: April 22, 2018)

We study far-from-equilibrium dynamics in models of freely cooling granular gas and ballistically aggregating compact clusters. For both the cases, from event driven molecular dynamics simulations we have presented detailed results on structure and dynamics in space dimensions $d = 1$ and 2 . Via appropriate analyses it has been confirmed that the ballistic aggregation mechanism applies in $d = 1$ granular gases as well. Aging phenomena for this mechanism, in both the dimensions, have been studied via the two-time density autocorrelation function. This quantity is demonstrated to exhibit scaling property similar to that in the standard phase transition kinetics. The corresponding functional forms have been quantified and discussed in connection with the structural properties. Our results on aging establish a more complete equivalence between the granular gas and the ballistic aggregation models in $d = 1$.

PACS numbers: 47.70.Nd, 05.70.Ln, 64.75.+g, 45.70.Mg

I. INTRODUCTION

Structure and dynamics during cooling in systems of inelastically colliding particles have been of much research interest [1–22]. An importance of this topic stems from the relevance of it in the agglomeration of cosmic dust [21]. Two models in this context have been of significant importance, viz., the granular gas model (GGM) and ballistic aggregation model (BAM). In the BAM, following a collision between two freely moving clusters, the colliding partners form a single larger object. In one dimension this corresponds to the sticky gas. While collisions trigger clustering immediately in the case of BAM, for the GGM (with coefficient of restitution $0 < e < 1$) the system remains in a homogeneous density state during an initial period, referred to as the homogeneous cooling state (HCS) [3, 18]. The dynamics in the latter then crosses over to an inhomogeneous cooling state (ICS) [3], where particle-poor and particle-rich domains emerge. Time scale for such a crossover gets shorter with the decrease of e . These domains or clusters may grow for indefinite period of time if the system size is thermodynamically large [22]. Thus, even if not a phase transition, it is quite natural to study clustering phenomena in these models from the perspectives of phase transition kinetics [23–25].

In problems of phase transitions [23], having been quenched from a homogeneous state to a state inside the miscibility gap, as a system proceeds towards the new equilibrium, one is interested in understanding the domain pattern [23], its growth [23] and aging [25]. Typically, a pattern is characterized via the two-point equal-time correlation function [23] C , which, in an isotropic situation, is calculated as [23] (r being

the scalar distance between two points)

$$C(r, t) = \langle \psi(\vec{r}, t) \psi(\vec{0}, t) \rangle - \langle \psi(\vec{r}, t) \rangle \langle \psi(\vec{0}, t) \rangle, \quad (1)$$

where ψ is a space (\vec{r}) and time (t) dependent order parameter. For a vapor-liquid transition, which granular systems have resemblance with, ψ is related to the local density. For a self-similar pattern, $C(r, t)$ and its Fourier transform, $S(k, t)$ (k being the magnitude of the wave vector), the structure factor, obey the scaling properties [23]

$$C(r, t) \equiv \tilde{C}(r/\ell), \quad S(k, t) \equiv \ell^d \tilde{S}(k\ell), \quad (2)$$

where \tilde{C} and \tilde{S} are time-independent master functions [23]. These dynamic scalings reflect the fact that structures at two different times are similar, apart from a change in length scale ℓ , the average size of domains, that grows with time as [23]

$$\ell \sim t^\alpha. \quad (3)$$

For the study of aging property, one considers a two-time autocorrelation function [26, 27]

$$C_{\text{ag}}(t, t_w) = \langle \psi(\vec{r}, t) \psi(\vec{r}, t_w) \rangle - \langle \psi(\vec{r}, t) \rangle \langle \psi(\vec{r}, t_w) \rangle, \quad (4)$$

where t_w ($\leq t$) is referred to as the waiting time or age of the system [25]. Unlike the equilibrium situation, the decay of $C_{\text{ag}}(t, t_w)$ gets slower with the increase of t_w , when plotted vs $t - t_w$, since there is no time translation invariance in an evolving system. In kinetics of phase transitions, $C_{\text{ag}}(t, t_w)$ follows a scaling relation [25, 26]

$$C_{\text{ag}}(t, t_w) \equiv \tilde{C}_{\text{ag}}(\ell/\ell_w), \quad (5)$$

where ℓ_w is the domain size at t_w and \tilde{C}_{ag} is a master function [25] that typically exhibits power-law decay

as a function of ℓ/ℓ_w . Examination of these facts for systems as nontrivial as those consisting of inelastic particles should be of genuine interest, to gain an universal picture of the concepts of nonequilibrium statistical mechanics, since these systems continuously dissipate kinetic energy.

Like in phase transitions, in the case of inelastic particles also, considered to be hard spheres in many theoretical studies, power-law growths have been observed [5, 8–11, 13]. In phase transitions, ℓ can be connected to the interfacial energy. Even though a connection with interfacial energy does not exist here, for the BAM the average cluster mass (m) has been related with the average kinetic energy (E) [21]. In many problems of coarsening, the growth exponent α depends upon the transport mechanism and system dimensions [23]. In the case of BAM also time-dependence of m has been predicted to have strong influence from dimension [21]. Despite these advancements, many questions remain open, including the issue related to the equivalence between BAM and GGM.

For the growth of m ($\sim \ell^d$, d being the system dimension) via the ballistic aggregation mechanism, a scaling theory predicts [21]

$$m \sim \frac{1}{E} \sim t^{\frac{2d}{d+2}}. \quad (6)$$

In $d = 1$, this has been confirmed via simulations, for both BAM and GGM cases [6, 7, 10, 11, 21]. In higher dimensions, on the other hand, the status is not satisfactory with respect to the equivalence between the two models. Even though the time-dependence of E is reported to be consistent with Eq. (6), for the growth of m in GGM, there exists evidence for dimension independence [13]. This raises question whether the complete validity of Eq. (6) in $d = 1$, for both BAM and GGM cases, is accidental. Thus, even in this dimension, direct confirmation of the mechanism for GGM is essential, to draw a conclusion on the equivalence [6] between the two models. For $d > 1$, strictly speaking, even for BAM, the time dependence in Eq. (6) requires modification, since in that case one expects isolated fractal clusters [28] with fractal dimension d_f ($< d$) such that $m \sim \ell^{d_f}$. This fact is not included in Eq. (6) and due to technical difficulties, in existing simulation studies also spherical (compact) structural assumption [14, 15] of the growing clusters became necessary.

Furthermore, while some aspects of kinetics have been studied, aging property [25–27, 29–33] of the density field and its connection to pattern and growth did not receive attention for these models, though important [34]. To the best of our knowledge, there exists only one study [35] that addresses scaling property of the two-time correlation function in the granular-matter context. This, however, considers aging in a

different quantity, for a model different from the one considered here.

Here note that various scaling properties that have been established with respect to aging are related to approach of a far-from-equilibrium system to an equilibrium state, like in phase transitions. Given that systems of inelastically colliding particles are always out of equilibrium, examination of the validity of these properties in such systems should be of fundamental importance. If scaling exists, it is of interest then to compare the scaling functions associated with GGM and BAM cases, to establish a more complete equivalence.

In this work, our primary objective is to identify the scaling property related to aging in ballistic aggregation. For this purpose, it has been shown, via a state-of-the-art dynamic renormalization group theoretical method of analysis [36], that the growth law for one-dimensional GGM in ICS is same as that for the BAM. In this dimension, we also directly show that the mechanism of aggregation in GGM is indeed ballistic. These, along with our results on aging, establish a more complete equivalence between GGM and BAM in $d = 1$. On the other hand, we have pointed out vast differences between the structure and dynamics of GGM and the corresponding theoretical expectations for $d = 2$ BAM. For the latter dimension, thus, for aging property we work only with the BAM. We show that, irrespective of the dimension, the above scaling property of the autocorrelation function holds for both the models as long as the growth occurs via ballistic aggregation. These results are discussed with reference to the picture in standard phase transitions. The functional forms of \tilde{C}_{ag} have been estimated and understood via analyses of the structure [29]. In $d = 2$, via accurate analyses, we also check the validity of a hyperscaling relation involving the decay of energy and growth of clusters for the BAM.

The rest of the paper is organised in the following way. We discuss the model and methods in Section II. The results are presented in Section III. Finally, Section IV concludes the paper with a summary and outlook.

II. MODEL AND METHODS

For the GGM we use the following update rule for (hard) particle velocities. The post and pre-collisional velocities of the particles are related via [3, 37, 38]

$$\vec{v}_i' = \vec{v}_i - \left(\frac{1+e}{2}\right)[\hat{n} \cdot (\vec{v}_i - \vec{v}_j)]\hat{n}, \quad (7)$$

$$\vec{v}_j' = \vec{v}_j - \left(\frac{1+e}{2}\right)[\hat{n} \cdot (\vec{v}_j - \vec{v}_i)]\hat{n}, \quad (8)$$

where ($'$) stands for the post event, \vec{v}_i and \vec{v}_j are velocities of particles i and j , respectively, and \hat{n} is the unit vector in the direction of the relative position of the particles i and j . With this model, we perform event driven [37, 38] molecular dynamics simulations where an event is a collision. In this method, between two collisions, since there are no inter-particle interaction or external potential, particles move with constant velocities till the next collision, which is appropriately identified after every event.

For the BAM case [21], following every collision, mass of the product particle increases, which was appropriately incorporated in the collision rule. For the BAM in $d = 2$ we use the same circular approximation of the product clusters as in the previous studies [39], which will be briefly discussed later. Typically, in such event driven simulations, time is specified in two different ways, viz., by using the number of collisions per particle (τ) and actual time (t), the latter being calculated by keeping track of the free time between successive collisions. In this work, we will use the latter.

A serious problem faced in event driven simulations of the GGM is the inelastic collapse [40]. This phenomenon is related to the fact that for very low values of the relative velocity collisions keep happening only among a small group of neighboring particles, thereby essentially providing no progress in time. The problem is more severe in lower dimension, since fewer particles are needed to satisfy the corresponding condition. There can be two ways to avoid such singularity in collision numbers, viz., setting the value of e , for the collision partners with relative velocities less than a threshold value δ , to either 0 or 1. We adopt the latter [6, 40–42] given that in the experimental situation value of e increases with the decrease of the relative velocity [10–12, 43]. In $d = 2$, however, we set δ to zero, since the problem is less severe in higher dimension and so, significantly large cluster sizes can be accessed without encountering such events.

All our results will be presented from simulations with periodic boundary conditions and density of particles starting with $\rho = N/L^d = 0.30$, N being the number of particles and L the linear dimension of the system, except for the $d = 2$ GGM for which we choose $\rho = 0.37$. Given that the particles have diameter unity (to start with), in $d = 2$ these numbers for particle density correspond to packing fractions 0.235 (BAM) and 0.29 (GGM).

In the case of GGM, clusters were appropriately identified as regions with density above a critical value ρ_c ($= 0.5$). Higher values of ρ_c also provide similar results, deviating from each other only by a multiplicative factor. The end to end distance for a cluster along any direction provides a cluster length (ℓ_c). In $d = 1$, the number of particles within these boundaries is the mass (m_c) of that cluster. In $d = 2$, one

needs to appropriately identify the closed boundaries of the clusters, to calculate the mass. For the BAM case, information on the cluster length and mass are contained in the particle radius. The average values of the above mentioned quantities were obtained from the first moments of the corresponding distributions. Ideally, ℓ should equal $m^{1/d}$, but in the case of GGM it takes time for a cluster to settle down to a particular density value. Thus, equality holds only at late time. For the calculation of the correlation functions and structure factors [8, 9], the order-parameter ψ at a point was assigned a value +1 if the density (calculated by counting the number of nearest neighbors) there was higher than ρ_c , else -1 . The average length can be calculated from the scaling property of $C(r, t)$ or $S(k, t)$ as well.

III. RESULTS

We divide the section into sub-parts **A** and **B**. In subsection **A** we present results from $d = 1$ and $d = 2$ results are shown in subsection **B**.

A. $d = 1$

As mentioned above, in this dimension, via accurate analyses, we first confirm an equivalence between the BAM and GGM, with respect to the energy decay, growth law and mechanism. These results are followed by those for aging property. As we will see, the latter, in addition to being of separate importance, will make the above mentioned equivalence more complete.

In Figure 1(a) we show the decay of energy, for both GGM and BAM, as a function of time, on a log-log scale. The BAM results, for energy and mass (see Figure 1(b)), are already understood. However, we present these for the sake of completeness, as well as to facilitate the discussion that follows. For the GGM, results for a few different cut-off values of the relative velocity are shown. For this case, in this dimension, all our results correspond to $e = 0.5$. After a minor disagreement over brief initial period (corresponding to HCS in the GGM), all the results are consistent with each other, exhibiting power-law behavior over several decades in time, with the expected exponent $-2/3$.

In Figure 1(b) we plot m as a function of t , on a log-log scale, for the BAM case. This shows a power-law growth with exponent $2/3$, validating Eq. (6). The m vs t results for the GGM are shown in Figure 1(c), for the same values of δ as in Figure 1(a). An interesting observation here is that, for the GGM, even though the energy decay follows $t^{-2/3}$ behavior till late for all values of δ , the picture is different for the

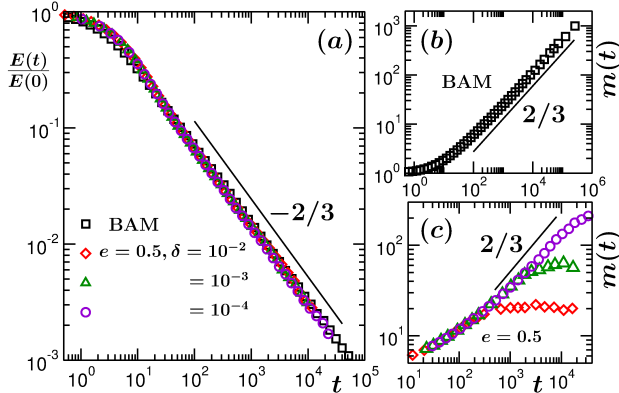


FIG. 1. (a) Plots of energy decay as a function of time, for BAM and GGM cases. For the GGM case, value of e has been fixed to 0.5 and results for several choices of δ are presented. (b) Average cluster mass, m , is plotted vs time, for BAM. (c) Same as (b) but for GGM with multiple values of δ as in (a). The solid lines in these figures correspond to various power-laws, exponents for which are mentioned. The starting number of particles for BAM and GGM are respectively 160000 and 10000. Rest of the simulations for GGM are done with 20000 particles and $\delta = 5 \times 10^{-5}$. All results are for $d = 1$.

growth of mass. The growth stops earlier for larger value of δ , even though energy decay continues with the predicted functional form. This should not be a finite-size effect, since the saturation is δ dependent. Rather, this has connection with late time declusterization phenomena [10, 11] that has been observed for relative velocity dependent e . Furthermore, the m vs t data, particularly for larger values of δ , do not appear consistent with the exponent $2/3$. This discrepancy can possibly be due to the presence of substantial length at the beginning of the scaling regime. In such a situation, confirmation of an exponent from a log-log plot requires data over several decades in time [44]. In absence of that, alternative accurate method of analysis is needed to obtain correct value of the exponent [36, 44, 45]. In any case, the observations above, with respect to the saturation of m , further justify the need for direct identification of the growth mechanism. Before moving to that we will accurately quantify the growth law. For this purpose, in the following we will work with the length rather than the mass, since for the aging property we will need this latter quantity. Unless otherwise mentioned, in this subsection, all our results for the GGM, from here on, will be presented for $\delta = 5 \times 10^{-5}$.

We use a renormalization-group method of analysis [36] for the accurate quantification of the growth for the GGM. We consider a Kadanoff type block transformation [46] of the order parameter. For this purpose, as mentioned in the context of calculation of

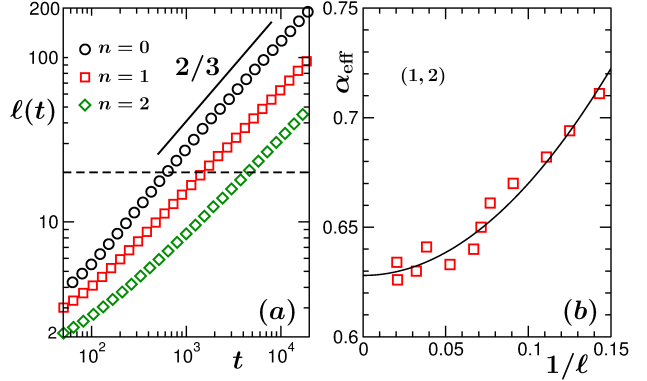


FIG. 2. (a) Plots of ℓ vs t for three different stages of renormalization. The dashed horizontal line is for the extraction of times for the same length at different levels of renormalization. The solid line represents a power-law with exponent $2/3$. (b) Plot of the effective exponent, obtained via the renormalization-group analysis using the combination $n = 1$ and 2 , vs the inverse of the original length. The solid line is a quadratic fit to the simulation data. All results correspond to the GGM in $d = 1$.

the correlation functions, we have mapped the density field to $\psi = \pm 1$. The blocking exercise then becomes similar to that for the Ising model [23]. At successive iterations of the transformation, order parameter over a length of b particle diameters is averaged over and represented by a single point, reducing the system size by a factor b , for which we choose the value 2. Thus, a particular value of ℓ in different levels (n) of renormalization will be obtained at different times, viz., for $n = p$ and $p + 1$ one writes [36]

$$\ell(p, t) = \ell(p + 1, b^{1/\alpha} t). \quad (9)$$

This is demonstrated in Figure 2(a), where, in addition to the original data ($n = 0$), we have presented length vs time plots for renormalizations with $n = 1$ and 2 . The horizontal line in this figure is related to the estimation of times for the same length scale for different values of n . From the shifting or scaling of time, due to the scaling in length, the growth exponent can be estimated. However, because of technical reasons the true exponent will be realized only in the limit $\ell \rightarrow \infty$ and for finite time we will denote it by α_{eff} .

Estimated values of α_{eff} , from the combination involving $n = 1$ and 2 , are presented in Figure 2(b), vs $1/\ell$, which indeed have time dependence [47]. The time dependence is due to the nonscaling early time transient and presence of a large off-set when scaling is reached. When such time dependence exits, as already stated, α should be estimated from the convergence of the data in the $\ell \rightarrow \infty$ limit. By looking at the trend of the data set, we have fitted it to the

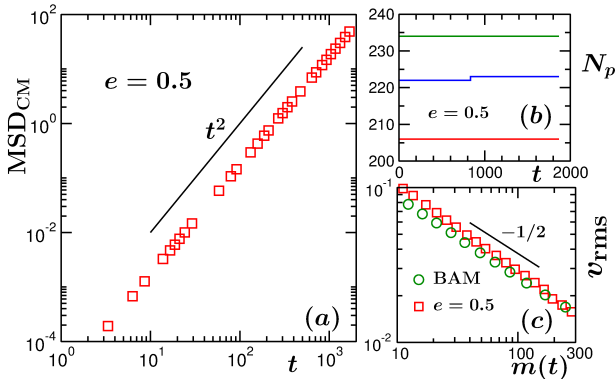


FIG. 3. (a) Mean-squared-displacement of the centre of mass of a typical cluster, for GGM, is plotted vs time, on a log-log scale. The solid line corresponds to ballistic motion. (b) Number of particles in a few different clusters, for GGM, are plotted vs translated time, before they undergo collisions. (c) Root-mean-squared velocity of the clusters are plotted vs m , for both BAM and GGM. The solid line is a power-law decay, exponent being mentioned. All results are from $d = 1$.

form $\alpha_{\text{eff}} = \alpha + a/\ell^2$, that provides convergence to $\alpha \simeq 0.63$. This is very close to the ballistic aggregation [21] value $2/3$. To check, whether this minor deviation of the simulation data from the theoretical expectation is a true fact, one needs to study other values of e as well. Such a systematic study we leave out for a future work. The deviation could be due to the finite-size effects and δ -dependent saturation.

Having identified the growth exponent for the GGM, we, in Figure 3, identify the mechanism. The growth exponent $2/3$ can be obtained from a (nonequilibrium) kinetic theory for ballistic aggregation [21, 28, 48]. As the name suggests, the growth occurs in this mechanism due to collisions among clusters and between collisions the clusters move with constant velocities. Since the particles in our models are noninteracting, it is understandable that the clusters in the BAM will move ballistically between collisions. In the GGM case also, following more and more collisions, particles within a cluster may move parallel to each other, providing collective directed motion. However, when a cluster moves through a vapor region, growth in this case may occur due to random deposition of particles on them. It is then necessary to check if at late enough time the motion of the clusters, during the interval between two big mass enhancing collisions, are ballistic and during that period the growth of the clusters is negligible.

In part (a) of Figure 3 we show the mean-squared-displacement of the centre of mass (CM), MSD_{CM} , of a cluster, calculated as [49]

$$\text{MSD}_{\text{CM}} = \langle |\vec{R}_{\text{CM}}(t) - \vec{R}_{\text{CM}}(0)|^2 \rangle, \quad (10)$$

\vec{R}_{CM} being the time-dependent location of the CM of the cluster, for GGM, over an extended period of time, before it undergoes a collision with another cluster. On the log-log scale, a very robust t^2 behaviour is visible, confirming ballistic motion [49]. In Figure 3(b) we show number of particles in a few clusters, as a function of translated time. The constant values over long time confirm that the mechanism of growth in the GGM is indeed ballistic aggregation.

The mass part of Eq. (6) can be derived from [21, 28, 48]

$$\frac{dn_c}{dt} = -\ell^{d-1} v_{\text{rms}} n_c^2, \quad (11)$$

where n_c is the cluster density and v_{rms} is the root-mean-squared velocity of the clusters. An exponent $2/3$ requires $v_{\text{rms}} \sim m^{-1/2}$, an outcome for uncorrelated cluster motion [48], can be realized for Boltzmann distribution of cluster kinetic energies [15, 28]. In Figure 3(c), we plot v_{rms} vs m , for BAM as well as GGM, both of which show reasonable consistency with the requirement. Here note that at low values of particle density, strong velocity correlation is expected to appear, since the collisions are less random, leading to deviation from such Boltzmann distribution picture. At high density, the collisions are random and such a picture is a good approximation. The reasonable validity of v_{rms} with the $m^{-1/2}$ form, that is observed, should, however, be checked for other values of e for the GGM to see if there exists complex density dependence. Any deviation, though does not invalidate the ballistic aggregation, can bring in change in the growth exponent. Here, as a passing remark, we mention that for the ballistic aggregation of fractal clusters in d dimensions, with $v_{\text{rms}} \sim m^{-\gamma}$, the exponent for the time dependence of mass will have the form

$$\zeta = \frac{d_f}{1 - d + d_f(1 + \gamma)}, \quad (12)$$

if Eq. (11) is a good starting point. Given that for the present problem $d_f = d = 1$ and our estimate of γ for the GGM is 0.55, $\zeta = 0.645$, in agreement with the conclusion from Figure 2(b). We obtain similar result for ζ via analysis of the instantaneous exponent. For $d = 2$, we will adopt this method, instead of the renormalization group.

Next we present results for the aging property [25, 26]. We stress again, not only in the granular matter context, to the best of our knowledge, aging has not been studied previously for ballistic aggregation in any other system. In Figure 4(a) we plot $C_{\text{ag}}(t, t_w)$ vs $t - t_w$, for a few different values of t_w , for the GGM. As expected, no time translation invariance is noticed which is an equilibrium [49] (or steady-state) property. Sticky gas (BAM) results are

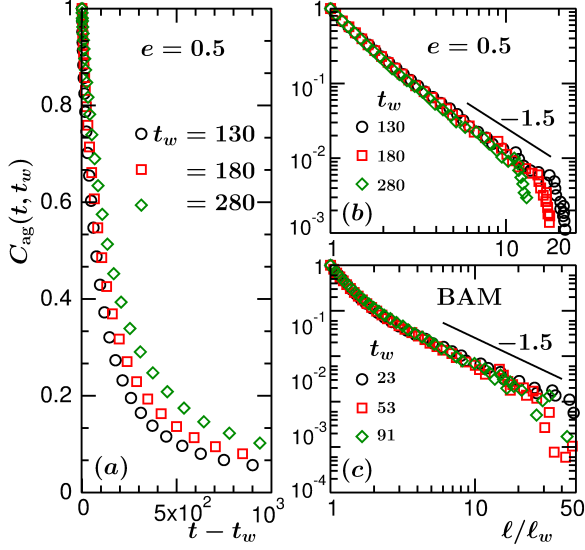


FIG. 4. (a) Plots of the autocorrelation function, vs $(t - t_w)$, for three different choices of t_w , as mentioned, for the $d = 1$ GGM. (b) Log-log plots of $C_{\text{ag}}(t, t_w)$ vs l/l_w , using the data sets in (a). (c) Same as (b) but for the $d = 1$ BAM case. The values of t_w are mentioned on the figure. The solid lines in (b) and (c) represent power-law decays with exponent $\lambda = 1.5$.

similar (not shown). In Figure 4(b) we show $C_{\text{ag}}(t, t_w)$ vs l/l_w , on a log-log scale, for the GGM. Nice collapse of data from all chosen values of t_w are seen, as in kinetics of phase transition. Deviations of the data sets from the master curve, appearing earlier for larger values of t_w , are due to finite-size effects [50]. In phase transitions, the system moves towards an equilibrium state. Interestingly, similar scaling is observed in the present case, despite the fact that the system is continuously dissipating kinetic energy. Corresponding plots for the BAM are shown in Figure 4(c). Again, very good quality collapse is observed. In both the cases, power-law decays [26]

$$\tilde{C}_{\text{ag}} \sim x^{-\lambda}; \quad x = l/l_w, \quad (13)$$

of the scaling function are observed for $x \gg 1$, the exponent value, mentioned on the figures, being same (or close to each other) in the two cases. This further confirms the equivalence between the BAM and the GGM.

In phase transitions, there exists a lower bound [26, 29] for the value of λ , viz.,

$$\lambda \geq \frac{d + \beta}{2}, \quad (14)$$

where β is the exponent for the small wave number

power-law behaviour of the structure factor:

$$S(k, t) \sim k^\beta. \quad (15)$$

The bound in (14) was derived by Yeung, Rao and Desai (YRD) [29]. For this purpose, starting from the structure factors at times t and t_w , YRD obtained

$$C_{\text{ag}}(t, t_w) \leq \ell^{d/2} \int_0^{2\pi/\ell} dk k^{d-1} [S(k, t_w) \tilde{S}(k\ell)]^{1/2}. \quad (16)$$

The bound follows when Eq. (15), for the small k behavior of $S(k, t_w)$, is used in the above expression. To check whether λ in the present case also obeys the bound (14), we analyze the structure.

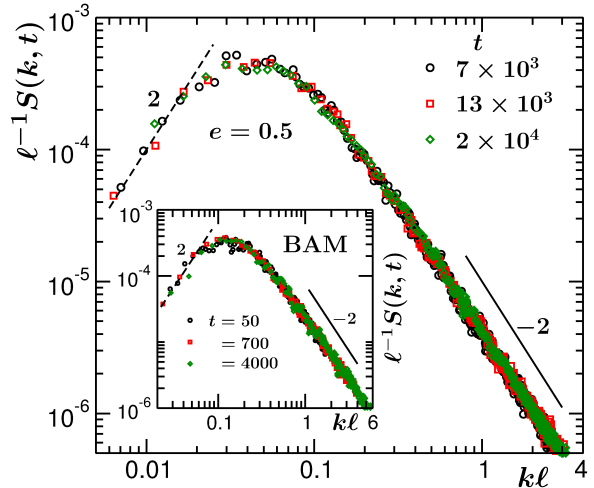


FIG. 5. Scaling plot of the equal-time structure factors for the $d = 1$ GGM. Here we have shown collapse of $S(k, t)/\ell(t)$, when plotted as a function of $y = k\ell(t)$, using data from three different times. Inset shows the same exercise as in the main frame but for $d = 1$ BAM. In the main frame as well as in the inset, the dashed and the solid lines correspond to $\sim y^2$ and $\sim y^{-2}$, respectively.

In Figure 5 we show the scaling plot of the structure factors, viz., we plot $\ell^{-1}S(k, t)$ vs $k\ell$, for the GGM. Nice collapse of data from all different times imply structural self-similarity [23]. The consistency of the long wave-vector data with k^{-2} imply validity of the Porod law [23, 51, 52]

$$S(k, t) \sim k^{-(d+1)}, \quad (17)$$

a consequence of short-distance singularity in $C(r, t)$, due to scattering from sharp interfaces. The small k behaviour appears consistent with $\beta = 2$. The behaviour for the BAM structure factor, shown in the inset of Figure 5, is very similar. This value of β was predicted [53] for coarsening in Ising-like systems in $d = 1$. The number is different for higher dimensions [54]. The dimension dependent values of β can

be obtained [55] from dynamical equation of structure factor (starting from the Cahn-Hilliard equation [55]) in k space, by arguing that for $d = 1$ thermal energy is dominant, whereas for $d > 1$ interfacial free energy takes over. Agreement of our results with such prediction is very interesting. The information on the consistency, for both short and long range structures, between GGM and BAM, that these data sets convey, is further supportive of the presence of sharp interfaces, compact clusters and ballistic aggregation in the GGM.

The observed value of β sets the lower bound for λ at 1.5. Thus, this bound is obeyed in both the cases and the actual values of the aging exponent in fact are very close to this lower bound. Here note that recently violation of such power-law decay of the auto-correlation function was demonstrated [32, 33] for advective transport in fluid phase separations. Even for conserved order parameter with diffusive dynamics, though power-law, the decays in $d > 1$ are observed [56] to be significantly faster than the ones provided by the the (lower) bound (14). However, in the latter example, agreement with the bound gets better as the dimension decreases [56]. With the lowering of d , particularly for Ising kinetics, motion of the boundaries of domains (during no growth periods) gets restricted. However, since the mechanism is ballistic in the present problem, boundary movement does exist even during no growth period, though decreases with the increase of mass, thus time. Nevertheless, the agreement with the lower bound is rather close.

B. $d = 2$

In this subsection, first we briefly discuss the case of GGM, to convince ourselves that the growth in this case does not occur via the ballistic aggregation mechanism. Unlike the simulations of GGM in $d = 1$, we do not use any nonzero cut-off value (δ) for the relative velocity here. This is because, for high enough value of e , in this dimension, we are able to access relevant scaling regime without encountering an inelastic collapse [13].

In Figure 6(a) we show an evolution snapshot for the $d = 2$ GGM with $e = 0.9$. Interesting pattern, with coexisting high and low particle-density domains, is visible. A log-log plot of the decay of kinetic energy for the system, as a function of t , is presented in Figure 6(b). The initial decay (corresponding to HCS) is consistent with the prediction of Haff [18], $E \sim e^{-at}$ (a is a constant; analytical curve is not shown). The late time data follow a power-law in t , with exponent -1 . This is, thus, consistent with the prediction of Eq. (6). In Figure 6(c) we show a log-log plot of m vs t . The data in the late time scaling regime are seen

to obey a power law, the exponent being $\lesssim 2/3$. Here we mention that in a previous work [13], via a finite-size scaling analysis, we had shown that the average domain length grows as t^α with $\alpha \simeq 1/3$. The conclusion from Figure 6(c) is thus in agreement with this earlier study. Nevertheless, given that for the GGM there exists possibility of continuous change of density within the domains, it is instructive to calculate the average mass [13].

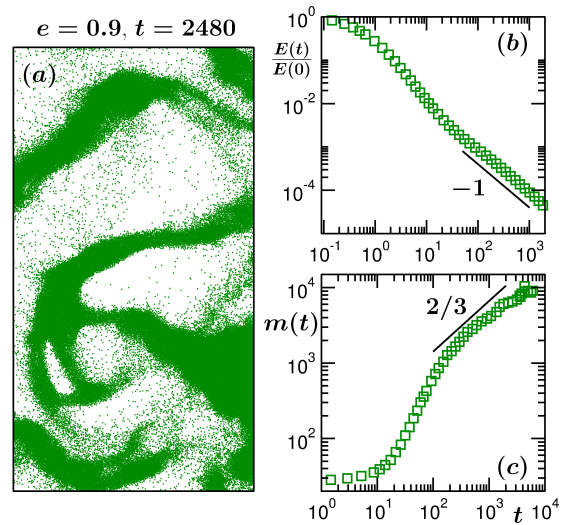


FIG. 6. (a) A snapshot during the evolution of GGM with $e = 0.9$ in $d = 2$. Only a part of the snapshot is shown. The particles are marked by dots. (b) Log-log plot of the energy decay as a function of t , for the system in (a). (c) Log-log plot of mass vs time, for the GGM in (a). All results are for $L = 512$. The solid lines in (b) and (c) represent power laws, exponents for which are mentioned.

Since Eq. (6) predicts inverse relationship between mass and energy, the kinetics of GGM is different from ballistic aggregation, particularly when the exponents do not follow even a hyperscaling relation [14, 15] (see discussion below in the context of BAM). Matching of the exponent for energy decay (with Eq. (6)) is accidental. In the rest of the subsection, therefore, we focus only on the BAM. This is by keeping the primary objective of studying aging during ballistic aggregation in mind.

There are different variants of models dealing with ballistic aggregation. E.g. there exists interest in a model where ballistically moving particles from a source get deposited on a fixed substrate or seed. Such models are of relevance in situations like construction of vapor-deposited thin films and the corresponding structures are fractal [57]. In the present case, however, all the clusters move ballistically, between collisions. Simulation of such BAM in $d > 1$ is not straight forward. If no deformation of the clusters is considered, highly fractal structures are expected

in this situation as well. In that case, one needs to keep track of the exact points of contact, when two clusters collide. This is a difficult task, particularly if the rotations of the clusters are considered. In the left frame of Figure 7(a) we show a snapshot, obtained during an evolution for the BAM, without incorporating any deformation and considering only the translational motion of the clusters. Nice fractal pattern is seen. We have estimated the fractal dimension which we discuss later.

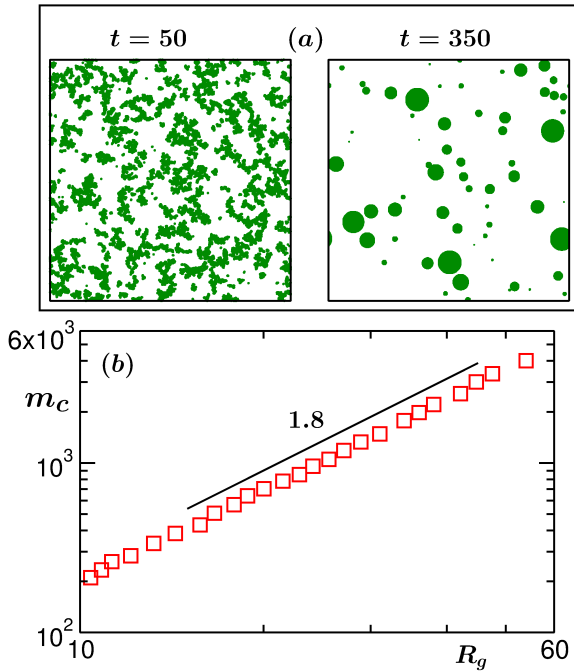


FIG. 7. (a) (Left frame) A snapshot during the evolution of the fractal BAM in $d = 2$ with $L = 512$. See text for details. (Right frame) Same as the left frame but with spherical structural approximation and for $L = 1024$. In both the frames only parts of the original systems are shown. Times are mentioned on top of the frames. (b) Cluster mass, from a typical snapshot, is shown as a function of the radius of gyration, R_g , for the fractal BAM case. The solid line there is a power-law with exponent 1.8. Rest of the results will be presented for $L = 1024$ and spherical BAM.

Because of the above mentioned difficulty in dealing with the actual physical scenario, researchers [14, 15, 39] have adopted a spherical structural approximation. In this method, after a collision between two spherical objects of diameters σ_1 and σ_2 , the mass of the resulting cluster is (usually uniformly) distributed over the volume of a sphere or circle (depending upon the system dimension) of diameter

$$\sigma = (\sigma_1^d + \sigma_2^d)^{1/d}. \quad (18)$$

Many materials are prone to permanent deformation

after high impact collisions. This is, thus, a reasonable approximation if the time scale of deformation is low, compared to the mean free time. In any case, given that fractality offers larger collision cross-section, the dynamics of the systems with such spherical structural approximation will be different from those without the approximation. In the rest of the subsection, unless otherwise mentioned, by BAM we will refer to the ballistic aggregation model with circular approximation.

In the BAM, the post-collisional position and velocity of a new cluster can be obtained from the conservation equations related to centre of mass and linear momentum. A snapshot during the evolution of a system with such rules is shown in the right frame of Figure 7(a). Before presenting results on dynamics of this simplified model, in Figure 7(b) we present result for the fractal dimension corresponding to the snapshot in the left frame of Figure 7(a). Here we show mass of individual clusters as a function of the radius of gyration (R_g), on a log-log scale. Nice power-law behavior is visible, providing (mass) fractal dimension $d_f \simeq 1.8$. As mentioned above, henceforth we will work with only the circular BAM. Even though the primary aim is to examine scaling property related to aging, in the following we present accurate results for energy decay and cluster growth as well, from appropriate analyses. To the best of our knowledge, such accurate analyses were not previously performed to draw conclusions on the behavior of these quantities.

In Figure 8(a) we show a log-log plot of energy decay as a function of time. A plot for the growth of mass is shown in Figure 8(b). Power laws in both the cases can be identified. While from these log-log plots it appears that the energy and mass are inversely proportional to each other, as predicted in Eq.(6), the inset of Figure 8(b), where we show kinetic energy as a function of mass, provides a different information. There the exponent of the power-law decay appears clearly higher than unity, approximately 1.15, over a significant range. For an accurate estimate we, thus, calculate the instantaneous exponents [45] for the time dependence of m and E as

$$\theta_i = -\frac{d \ln E}{d \ln t}, \quad \zeta_i = \frac{d \ln m}{d \ln t}. \quad (19)$$

Such exercises were performed for the $d = 1$ BAM as well. However, we avoided presenting those results, since this aspect in $d = 1$ is better understood.

We have plotted θ_i , vs $1/t$, and ζ_i , vs $1/m$, in Figures 9 (a) and (b), respectively. In the asymptotic limit we obtain $\theta \simeq 1.08$ and $\zeta \simeq 0.94$. Thus, the predictions of Eq. (6) are not obeyed. These numbers, however, appear consistent with a hyper-scaling relation [15] in $d = 2$ (for ballistic aggregation):

$$\theta + \zeta = 2. \quad (20)$$

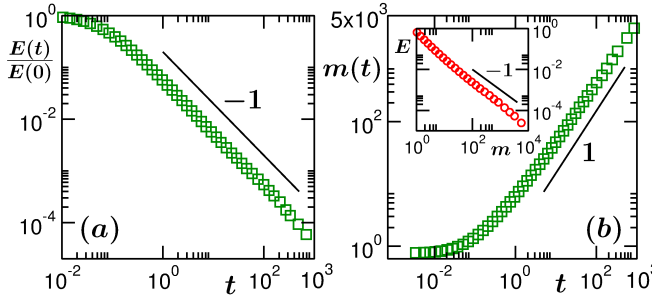


FIG. 8. Log-log plots of the (a) kinetic energy vs time and (b) mass vs time, for the $d = 2$ BAM. The solid lines in these figures are power-laws with exponents -1 and 1 , respectively. In the inset of (b) we show a log-log plot of E vs m . The solid there is a power-law with exponent -1 .

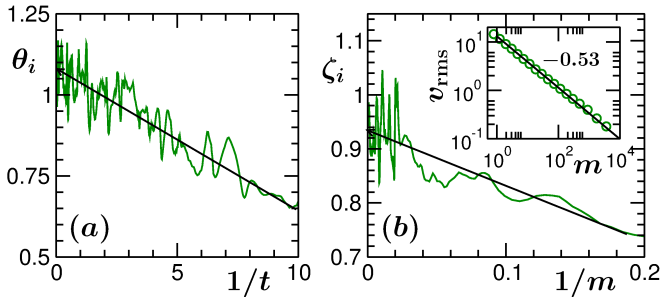


FIG. 9. Plots of (a) θ_i vs $1/t$ and (b) ζ_i vs $1/m$, for the $2D$ BAM. The solid lines are guides to the eye. Inset in (b): Log-log plot of v_{rms} vs m , for the $2D$ BAM. The solid line there is a power-law, exponent for which is mentioned next to it.

The failure of Eq. (6) lies in the fact that at low packing fraction the assumption related to uncorrelated velocity, inherent in the derivation of Eq. (6), breaks down [16]. It is expected that at higher density, where the collision events are more frequent, this prediction will work [15, 16, 39]. Here we ask the question is it not possible to obtain the above mentioned value of ζ from Eq. (11) or (12)? Note that under the spherical approximation $d_f = 2$. Thus, we need to estimate γ to find out the reason for deviation of ζ from unity (see Eq. (6)).

In the inset of Figure 9(b) we plot v_{rms} as a function of m . A power-law behavior from the log-log plot can be appreciated. The corresponding exponent ($\gamma \simeq 0.53$) provides $\zeta \simeq 0.97$ (see Eq. (12)). Even though this number is smaller than 1, no conclusive remark should be made from such small deviation. Following Ref. [16], we state here the reason behind a deviation between θ and ζ . Via the introduction of a dissipation parameter (α'), ratio between kinetic energy dissipation in a collision and mean kinetic energy per particle, these authors showed that $\alpha' = 1$

for high collision frequency. On the other hand, for low frequency, i.e., at low particle density, $\alpha' > 1$. In the latter scenario, the particles with larger kinetic energy than the mean undergo more frequent collisions, enhancing the dissipation. This leads to a value of θ higher than unity. This fact becomes more prominent at densities smaller than the one considered here. E.g., for $\rho = 0.005$, we find $\theta \simeq 1.15$ and $\zeta \simeq 0.85$. Similar fact is observed in $d = 3$. There, in future, we intend to verify how well the corresponding hyper-scaling relation [15] holds. Next we present results for aging.

In Figure 10(a) we show plots of $C_{\text{ag}}(t, t_w)$, vs $t - t_w$, for a few different values of t_w . Like in $d = 1$, time translational invariance is absent, as expected. It is clearly seen that with increasing age relaxation gets slower. In Figure 10(b) we show the log-log plots of $C_{\text{ag}}(t, t_w)$ as a function of ℓ/ℓ_w . Very nice collapse of data on a master curve is visible. This confirms the scaling property of Eq. (5). For large values of ℓ/ℓ_w power-law decay becomes prominent. Continuous bending of the master curve for small abscissa variable implies early-time correction to the power-law. The large x data appear to be consistent with an exponent $\lambda \simeq 1.6$, the number being roughly the same as in the $d = 1$ case. For aging in kinetics of phase transitions, on the other hand, one observes strong dimension dependence of λ [50, 56]. Here note that in $d = 2$ we expect [54] $\beta = 4$. Thus, the (lower) bound in (14) is 3. This calls for a look at the behavior of the equal-time structure factor for the present problem. While for bicontinuous domain structures ($d > 1$) the analytical prediction ($\beta = 4$) has been numerically confirmed [54, 58], the cases of discrete domain morphology are less studied. Before taking a look at the equal time structure factor, since a violation of the bound appears to be a possibility, in the inset of Figure 10(b) we plot the instantaneous exponent

$$\lambda_i = -\frac{d \ln C_{\text{ag}}}{d \ln x}, \quad (21)$$

as a function of $1/x$, to accurately quantify λ . The data set provides an asymptotic value $\lambda \simeq 1.55$.

In Figure 11 we present a scaling plot of $S(k, t)$, viz., we show $\ell^{-2} S(k, t)$ vs $k\ell$, on a log-log scale. The large k data are consistent with the power-law exponent -3 , that corresponds to the Porod law [51] in $d = 2$ for a scalar order parameter. In the small k region, on the other hand, the enhancement is much weaker than k^4 . In fact, in the relevant region, we observe $\beta \lesssim 1$. Similar number we have observed in recent studies of kinetics of phase transition with conserved off-critical composition as well, for which one naturally obtains circular or spherical domain structures. In that case we have the lower bound to be

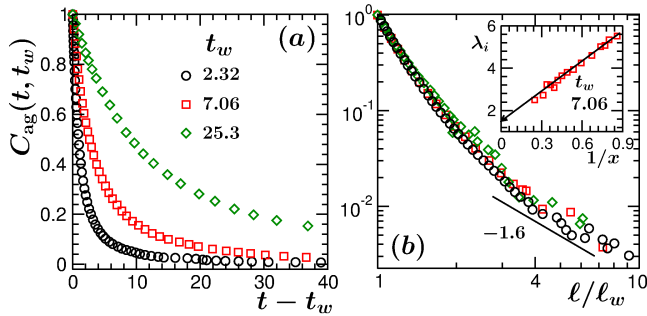


FIG. 10. (a) For the 2D BAM the autocorrelation function $C_{\text{ag}}(t, t_w)$ is plotted vs $t - t_w$. Results from three different t_w values are included. (b) Log-log plot of $C_{\text{ag}}(t, t_w)$ vs $x (= l/l_w)$, using data sets of (a). The solid line represents a power-law with exponent $\lambda = 1.6$. In the inset of (b) we show the instantaneous exponent λ_i as a function of $1/x$. The solid line there is a linear extrapolation to $x = \infty$.

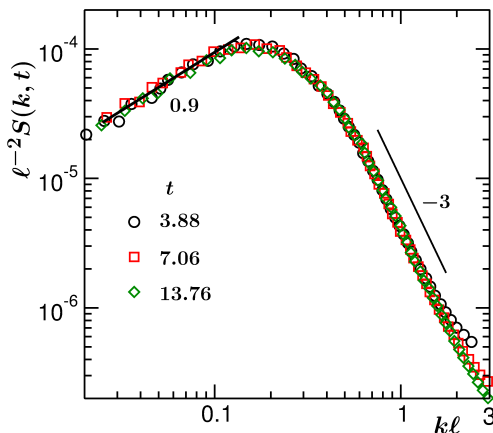


FIG. 11. Log-log plot of $l^{-2} S(k, t)$ vs kl , for the BAM in $d = 2$. The solid lines are power laws, exponents for which are mentioned on the figure.

$\lesssim 1.5$, which is satisfied by the above estimated value of λ .

IV. CONCLUSION

We have studied the kinetics of clustering in models of granular gas (GGM) and ballistic aggregation (BAM), in $d = 1$ and 2. It is shown that the average size of the clusters grows as power-law with time. In $d = 1$, via a dynamic renormalization group theoretical method of analysis [36], the exponent for the GGM has been identified to be approximately $2/3$, in agreement with that for the BAM. In this dimension, for

GGM as well as BAM, the growth appears inversely proportional to the energy decay, showing consistency with the scaling predictions of Carnevale *et al.* [21] for ballistic aggregation. The growth mechanism, for the GGM case, has been identified directly by calculating the mean-squared-displacements [49] of the centres of mass of clusters before they undergo collisions. To avoid the inelastic collapse, for the GGM, in this dimension, we have used a cut-off δ . For relative velocities $< \delta$, the value of e was set to unity for the colliding partners [6]. We observed δ -dependent saturation in the growth of mass, appearing earlier for larger values of δ . Interestingly, in such saturation regime also the energy decay continued to follow the theoretical scaling form $t^{-2/3}$. This calls for further investigation. In $d = 2$, on the other hand, any equivalence between GGM and BAM is shown to be absent.

In both the dimensions, for the density field, we have studied the aging property [25, 26] for ballistic aggregation, which is first in the literature. It is shown that, like in kinetics of phase transitions, the order-parameter autocorrelation function scales with l/l_w . The asymptotic forms of the scaling functions have been identified to be power-laws. The corresponding exponents have been estimated and discussed with reference to the structural property. It is shown that the exponents obey dimension dependent lower bounds, [29] predicted for kinetics of phase transitions where systems move towards a new equilibrium. However, unlike in the kinetics of phase transitions, the aging exponents here appear to be very close to the lower bounds, irrespective of the dimension. The similar values of the exponent for the GGM and the BAM cases in $d = 1$, further suggests close equivalence between the dynamics in the two cases, in this dimension. We intend to undertake similar studies in $d = 3$.

With respect to the more realistic ballistic aggregation, the simulations are rather challenging for $d > 1$. This is because of the formation of fractal structures. Because of this reason, like in the existing simulation studies, spherical structural approximation has been used by us. It will be interesting to investigate the scaling properties related to aging and other aspects without such approximation.

Acknowledgment: The authors thank Department of Science and Technology, India, for financial support. SKD also acknowledges the Marie Curie Actions Plan of European Commission (FP7-PEOPLE-2013-IRSES grant No. 612707, DIONICOS) as well as International Centre for Theoretical Physics, Trieste, for partial supports. SP is thankful to UGC, India, for research fellowship.

* das@jncasr.ac.in

-
- [1] I. S. Aranson and L. S. Tsimring Rev. Mod. Phys. **78** 641 (2006).
- [2] N.V. Brilliantov and T. Poeschel *Kinetic Theory of Granular Gases* (Oxford: Oxford University Press) (2004).
- [3] I. Goldhirsch and G. Zanetti, Phys. Rev. Lett. **70** 1619 (1993).
- [4] R. Brito and M. H. Ernst, Europhys. Lett. **43** 497 (1998).
- [5] S. Luding and H.J. Herrmann, Chaos **9** 673 (1999).
- [6] E. Ben-Naim, S.Y. Chen, G.D. Doolan and S. Render, Phys. Rev. Lett. **83** 4069 (1999).
- [7] X. Nie, E. Ben-Naim and S. Chen, Phys. Rev. Lett. **89** 204301 (2002).
- [8] S.K. Das and S. Puri, Europhys. Lett. **61** 749 (2003).
- [9] S.K. Das and S. Puri, Phys. Rev. E **68** 011302 (2003).
- [10] M. Shinde, D. Das and R. Rajesh, Phys. Rev. Lett. **99** 234505 (2007).
- [11] M. Shinde, D. Das and R. Rajesh, Phys. Rev. E **84** 031310 (2011).
- [12] A. Bodrova, A.K. Dubey, S. Puri and N.V. Brilliantov, Phys. Rev. Lett. **109** 178001 (2012).
- [13] S. Paul and S.K. Das, EPL **108** 66001 (2014).
- [14] E. Trizac and J.-P. Hansen, Phys. Rev. Lett. **74**, 4114 (1995).
- [15] E. Trizac and J.-P. Hansen, J. Stat. Phys. **82**, 1345 (1996).
- [16] E. Trizac and P.L. Krapivsky, Phys. Rev. Lett. **91**, 218302 (2003).
- [17] A. Lipowski, D. Lipowska and A. L. Ferreira, Phys. Rev. E **73**, 032102 (2006).
- [18] P. K. Haff, J. Fluid Mech. **134**, 401 (1983).
- [19] O. Herbst, R. Cafiero, A. Zippelius, H. J. Herrmann and S. Luding, Phys. of Fluids **17**, 107102 (2005).
- [20] S. Ulrich and A. Zippelius, Phys. Rev. Lett. **109**, 16601 (2012).
- [21] G.F. Carnevale, Y. Pomeau and W.R. Young, Phys. Rev. Lett. **64** 2913 (1990).
- [22] M. Hummel and M.G. Mazza, Phys. Rev. E **93** 022905 (2016).
- [23] A.J. Bray, Adv. Phys. **51:2** 481 (2002).
- [24] A. Onuki, *Phase Transition Dynamics* (UK: Cambridge University Press) (2002).
- [25] M. Zannetti, in *Kinetics of Phase Transitions*, ed. S. Puri S. and V. Wadhawan (Boca Raton: CRC Press) (2009).
- [26] D.S. Fisher and D.A. Huse, Phys. Rev. B **38** 373 (1988).
- [27] F. Liu and G.F. Mazenko, Phys. Rev. B **44** 9185 (1991).
- [28] J. Midya and S.K. Das, arXiv: 1604.06227 (2016).
- [29] C. Yeung, M. Rao and R.C. Desai, Phys. Rev. E **53** 3073 (1996).
- [30] M. Henkel, A. Picone and M. Pleimling, EPL **68** 191 (2004).
- [31] F. Corberi, E. Lippiello, A. Mukherjee, S. Puri and M. Zannetti, Phys. Rev. E **85** 021141 (2012).
- [32] S. Ahmad, F. Corberi, S.K. Das, E. Lippiello, S. Puri and M. Zannetti, Phys. Rev. E **86** 061129 (2012).
- [33] S. Majumder and S.K. Das, Phys. Rev. Lett. **111** 055503 (2013).
- [34] M. Hummel, J.P.D. Clewett and M.G. Mazza, EPL **114** 10002 (2016).
- [35] A. Baldassari, U.M.B. Marconi and A. Puglisi, Phys. Rev. Lett. **65** 051301 (2002).
- [36] C. Roland and M. Grant, Phys. Rev. B **41** 4663 (1990).
- [37] M.P. Allen and D.J. Tildesley, *Computer Simulation of Liquids* (Oxford: Clarendon) (1987).
- [38] D.C. Rapaport, *The Art of Molecular Dynamics Simulations* (Cambridge, England: Cambridge University Press) (2004).
- [39] S.N. Pathak, Z. Jabeen, D. Das and R. Rajesh, Phys. Rev. Lett. **112**, 038001 (2014).
- [40] S. McNamara and W.R. Young, Phys. Rev. E **50** R28 (1994).
- [41] C.S. Campbell, Annu. Rev. Fluid Mech. **22** 57 (1990).
- [42] S. Luding and S. McNamara, Gran. Matter **1** 113 (1998).
- [43] C.V. Raman, Phys. Rev. **12** 442 (1918).
- [44] S. Majumder and S.K. Das, Phys. Rev. E **81** 050102 (2010).
- [45] D.A. Huse, Phys. Rev. B **34** 7845 (1986).
- [46] N. Goldenfeld, *Lectures on Phase Transitions and the Renormalization Group* (Addison-Wesley) (1992).
- [47] S.K. Das and S. Puri, Phys. Rev. E **65** 26141 (2002).
- [48] S.N. Pathak, D. Das and R. Rajesh, EPL **107** 44001 (2014).
- [49] J.-P. Hansen and I.R. McDonald, *Theory of Simple Liquids* (London: Academic Press) (2008).
- [50] J. Midya, S. Majumder and S.K. Das, J. Phys.: Condens. Matter **26** 452202 (2014).
- [51] G. Porod, Small-Angle X-Ray Scattering, ed. O. Glatter and O. Kratky (New York: Academic Press) (1982).
- [52] Y. Oono and S. Puri, Mod. Phys. Lett. B **2**, 861 (1988).
- [53] S.N. Majumdar, D.A. Huse and B.D. Lubachevsky, Phys. Rev. Lett. **73** 182 (1994).
- [54] C. Yeung, Phys. Rev. Lett. **61** 1135 (1988).
- [55] H. Furukawa, Phys. Rev. B **40**, 2341 (1989).
- [56] J. Midya, S. Majumder and S.K. Das, Phys. Rev. E **92** 022124 (2015).
- [57] P. Ramanlal and L.M. Saner, Phys. Rev. Lett. **54**, 1828 (1985).
- [58] S. Ahmad, S.K. Das and S.Puri, Phys. Rev. E **85**, 031140 (2012).